

Article

# Experimental Investigation on the Mechanical Behavior of an Innovative Parabolic Trough Collector

Andrea Gilioli <sup>1</sup>, Luca Abbiati <sup>1</sup>, Massimo Fossati <sup>1</sup>, Francesco Cadini <sup>1</sup>, Andrea Manes <sup>1,\*</sup>, Marco Giglio <sup>1</sup>, Lino Carnelli <sup>2</sup>, Claudio Boris Volpato <sup>2</sup> and Stefano Cardamone <sup>2</sup>

<sup>1</sup> Mechanical Engineering Department, Politecnico di Milano, via La Masa 1, 20156 Milano, Italy; andrea.gilioli@polimi.it (A.G.); lucavincenzo.abbiati@mail.polimi.it (L.A.); massimo.fossati@polimi.it (M.F.); francesco.cadini@polimi.it (F.C.); marco.giglio@polimi.it (M.G.)

<sup>2</sup> Eni S.p.A., Renewable Energy & Environmental R&D Center, Istituto Eni Donegani, via Fauser 4, 28100 Novara, Italy; lino.carnelli@eni.it (L.C.); claudio.volpato@eni.com (C.B.V.); stefano.cardamone@eni.com (S.C.)

\* Correspondence: andrea.manes@polimi.it; Tel.: +39-02-2399-8630

Received: 3 October 2019; Accepted: 19 November 2019; Published: 21 November 2019



**Abstract:** In the present work an experimental program aimed at assessing the mechanical behavior of an innovative parabolic solar trough is presented. More specifically, a lightweight and low-cost collector making large use of adhesive joints, which can be easily assembled on-site, still performing at a high efficiency, was designed. Static and fatigue tests were performed on a full-scale prototype of the collector in the pre-production stage. The tests included differential torsion, concentrated and distributed bending, and distributed load (wind effect). During the tests, a network of strain gauges was placed in the most critical locations to measure the strain field, while laser sensors and cable transducers were placed in strategic positions to measure the displacements. The results demonstrate the strengths of the innovative parabolic trough collector and support the assessment of its structural integrity.

**Keywords:** renewables; solar energy; concentrated solar power system; experimental tests; structural integrity

## 1. Introduction

Concentrated solar power systems (CSP) represent very promising sources for the sustainable production of energy and, consequently in recent years, many efforts have been made by industrial companies and academic researchers to render this technology more and more profitable [1]. CSP systems convert solar power by using mirrors, or lenses, to reflect and concentrate a large amount of sunlight onto a receiver, which in turn collects and transfers the solar energy to a heat transfer fluid, which can be used to supply heat for end-user applications, to generate electricity by means of conventional steam turbines, and in many other applications [2,3]. The CSP receiver is a critical complex component and its thermal performances have been extensively studied in literature [4–7]. Even though the intuition at the base of the CSP technology is traditionally attributed to Archimedes back in 212 B.C. [8], in 2014, only approximately 5 gigawatts worldwide were generated by means of this technology. The main reason why CSP systems are still not used on a large scale is related to their still non-competitive costs, which are well described by the parameter “levelized cost of electricity” (LCOE), which summarizes an economical assessment of the average total cost to build and operate a power-generating asset over its lifetime, divided by the total energy output of the asset over that lifetime. It turns out that the LCOE of CSPs is high compared to other energy production

technologies, as reported for example in References [9,10]. According to References [11,12], the costs of the construction of the collector itself are mainly responsible for the still relatively high LCOE values.

In this context, the main objective of the present work was to assess the structural integrity and the mechanical behavior of an innovative lightweight and low-cost parabolic collector. The target of cost reduction means that the parabolic collector is supposed to be easily assembled on-site, using a reduced amount of pre-assembled components (that otherwise have to be shipped in the assembly location). Pre-assembled components in a highly specialized industrial environment warrant the achievement of the delivered mechanical behavior. On the contrary, full on-site manufacturing poses some challenges for the achievement of the following desired performance: High levels of efficiency, in spite of its lightness, with a potential to reduce the LCOE. The design of this structure, initially devised at Massachusetts Institute of Technology (MIT) [13] and developed by Eni in collaboration with Politecnico di Milano and MIT, was driven by a general cost reduction approach in terms of materials, production, transportation, assembly, and maintenance. Consequently, the rigorous assessment of the structural integrity of this system plays a fundamental role. The main idea behind this new design concept is inherited from the aeronautical engineering field, in which structures must be very light, but, at the same time, must also guarantee excellent reliability. The most innovative aspects of the design are the large use of adhesive joints and the almost complete absence of welds, rivets, and bolts. This design approach is expected to significantly reduce the weight and the construction time, but, due to its high level of novelty, requires an accurate assessment of its structural reliability.

Finally, it is worth mentioning that the present work shows a significantly innovative activity, since experimental tests of parabolic trough collectors in the literature are usually aimed at the assessment of the thermal efficiency of the system [14,15], especially with reference to the behavior of the fluid inside the receiver in the operating conditions of the plant [16]. As far as the authors know, no detailed studies to define the mechanical behavior and structural performances of a parabolic trough collector by means of an experimental activity on a full-scale prototype are present in the literature.

The article is divided into sections. In Section 2, a brief description of the main collector structural features is reported. Section 3 describes the experimental activities. The conclusions are reported in Section 4.

## 2. Materials and Methods

### 2.1. Collector Design Overview

The design of this structure was initially devised at Massachusetts Institute of Technology (MIT) [13] and developed by Eni in collaboration with Politecnico di Milano and MIT. One of the peculiar aspects of the trough design is the presence of seven curved ribs to which the mirror is joined (Figure 1). Analyzing the various solutions on the market [17,18], it is clear that no other design is similar to the one analyzed here. Indeed, the main structural solutions adopted by the competitors in recent years comprise the use of torque tubes or torque boxes placed on the rear side of the collector [19,20], which are not present here. In order to highlight the innovation of the present structure, the main components of the parabolic trough are shown in Figure 1. The incorporated stiff ribs allow the use of long steel panels (Figure 2) that span the entire length of the trough, which support the reflective film. At the connections between each panel, where the mirror surface is interrupted, the detrimental effects of the joints on the optical efficiency are reduced using few, but long, panels, which significantly reduce the number of discontinuities. In the present design, the use of bolt and rivet joints is limited, to the advantage of a large adoption of adhesively glued joints. The use of adhesive joints as a replacement for the bolt and rivet ones was previously investigated in References [21,22], where the authors demonstrated that the standards related to the strength and the stiffness can be fulfilled, as synthetically shown by the tensile strength comparison in Figure 3.



Figure 1. Main components of the parabolic trough collector.



Figure 2. (a) Overview of the parabolic trough collector prototype; (b) Side view of the trough rotated at  $-110^\circ$  and its support structure; (c) Detail of the shaft and the torsional strain gauges.

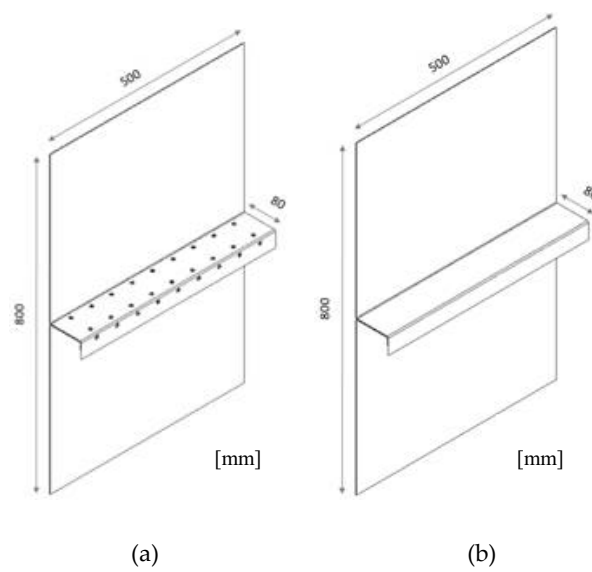
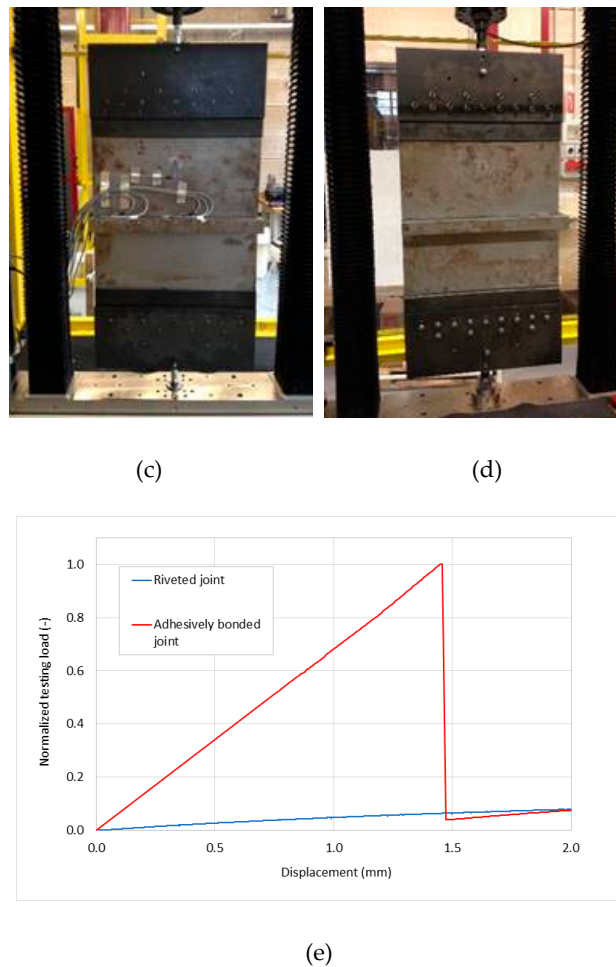


Figure 3. Cont.



**Figure 3.** Tensile strength comparison: Bolt joint (a) and (c) vs. adhesive joint (b) and (d) experimental setups and the results of the displacement-controlled tests (e).

On the basis of a cost/benefit analysis, construction steel was chosen as the building material.

Examples in literature demonstrating the application of the existing standards and codes to the design phase of a trough are reported in References [23,24].

## 2.2. Experimental Activity

The experimental activities performed on the prototype were aimed at investigating the structural performance (torsional stiffness, maximum rotation range) and the reliability of the trough when subjected to loads larger than the maximum usually encountered during its regular service. The experimental program can be classified into three different categories as follows:

- Movement tests (Section 2.2.2), aimed at verifying that the trough can cover the desired operational angle range in an adequate time;
- Static tests (Section 2.2.3), aimed at evaluating that under severe loads the trough does not fail and does not present excessive deformations;
- Fatigue test (Section 2.2.4), aimed at evaluating that after a cyclic severe load, the structure integrity of the trough is still guaranteed.

### 2.2.1. Experimental Setup

Two main typologies of measurement instruments were employed during the experimental phase, which were adopted to assess the behavior of the collector both on a global and local scale, as follows:

- Laser sensors (Figure 4a);
- Cable-extension position transducer (Figure 4b).

The global behavior of the trough refers, in particular, to the measurement of the displacement and stiffness of the trough, while the local behavior refers to the local measurement of the strain. The technical specifications of the adopted laser instruments are shown in Table 1.

**Table 1.** Technical specifications of the laser instruments.

<b>Ranging Unit</b>	• Unambiguity Interval: 153.49 m (503.58 ft)				
	• Range Focus <sup>3DS</sup> 120: 0.6 m–120 m indoor or outdoor with low ambient light and normal incidence to a 90% reflective surface				
	• Range Focus <sup>3DS</sup> 120: 0.6 m–20 m at normal incidence on 10% matte reflective surface				
	• Measurement speed (pts/sec): 122,000/ 244,000/ 488,000/ 976,000				
	• Ranging error: ±2 mm at 10m and 25m, each at 90% and 10% reflectivity				
<b>Ranging Noise</b>	@10m	@10m noise compr.	@25m	@25m noise compr.	
	@90% refl.	0.6 mm	0.3 mm	0.95 mm	0.5 mm
	@10% refl.	1.2 mm	0.6 mm	2.20 mm	1.1 mm
<b>Laser (Optical transmission)</b>	• Laser power (cw $\theta$ ): 20 mW (laser class 3R)				
	• Wavelength: 950 nm				
	• Beam divergence: Typical 0.19 mrad (0.011°)				
	• Beam diameter at exit: Typical 3.0 mm, circular				

The choice to use a more redundant measurement system was due to the large size of the prototype, which hampers the acquisition of good measurements using the laser instruments in particular (some positions are, in fact, difficult for the instruments to reach). Moreover, various configurations of the measurement layout (instrument positions, auxiliary structures) were used, depending on the different loading conditions under investigation.

In general, for almost all of the tests, two transducer cables were used to measure the displacements of the upper parts of the structure (dedicated structures were built to allow the wire to reach the points of interest on the prototype). In fact, it is worth remembering that the height of the trough can reach 7 m, thus making measurements on the top vertexes difficult. With regards to the lower part of the structure, laser sensors were adopted, since they could be placed in the correct position using very simple and mobile structures.

In order to acquire an overall knowledge of the local strain state in the parabolic trough, a network of 40 strain gauges (SG) were placed on it. More specifically, three different typologies of strain gauges were used, as follows:

- Uniaxial strain gauges, used to measure the strain on a single direction (37 linear SG LY11-6/120);
- Rosette strain gauge, composed of three strain gauges placed at different angles, two orthogonal and one at 45°, used to measure the full strain state on the surface of a part (1 rosette SG RY11-6/120);
- Torque strain gauges, used to measure the shear strain in order to obtain the torque applied to the trough (2 rosette SG XY21-6/120).

Since different typologies of tests were performed, characterized by various load cases, the most stressed areas were indeed always different. Therefore, several SGs were placed in order to be able to measure the strains at the critical locations for each load condition, however not all the SGs provided useful measurements during each test. Finally, two absolute optical rotary encoders, mounted on the rotating shafts on the sides of the trough, were used to measure the absolute rotation angle of the collector.

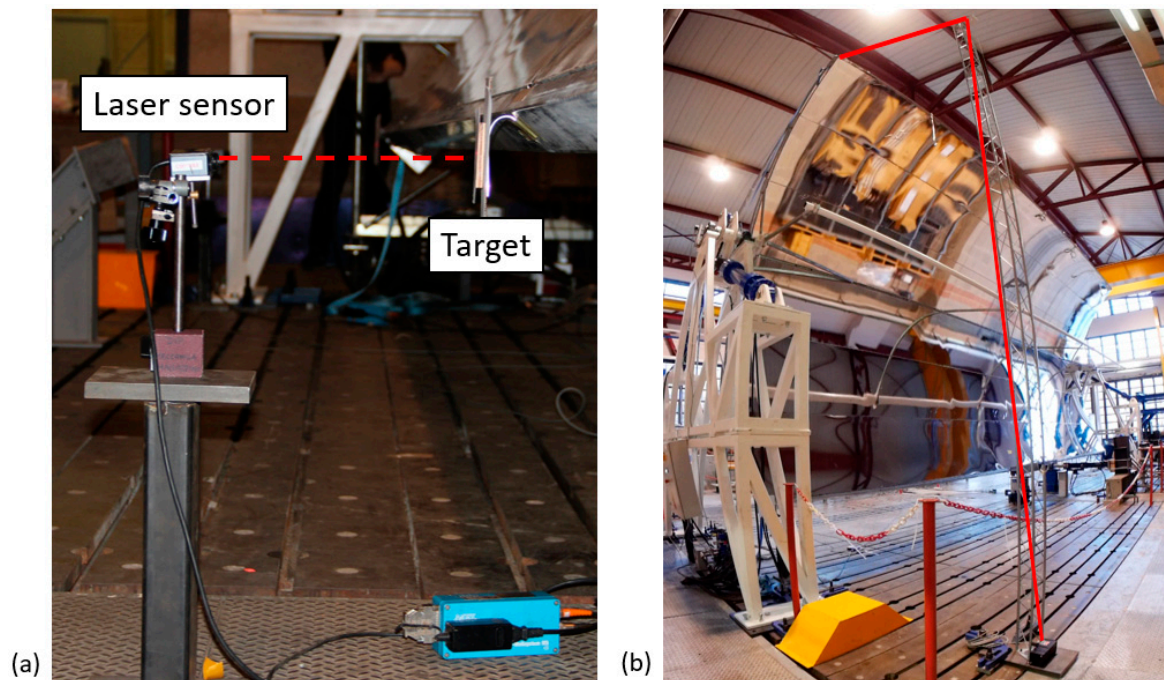


**Figure 4.** (a) Laser sensor on the support structure; (b) Overview of the turret adopted for the cable transducers (the cable is highlighted in red).

### 2.2.2. Movement Tests

In order to study the behavior of the parabolic trough under service conditions, the possibility of rotating the collector over a large angular range from  $-110^\circ$  to  $+110^\circ$  was checked (Figure 5). In addition to that, for safety reasons, the time required to rotate the solar trough from an in-service position to a safety recovery position ( $110^\circ$ ) was evaluated. For example, during service, if the wind speed reaches a critical value, the collector must be commanded to rotate to quickly reach a safety position, in which the winds can only load the back side of the trough.

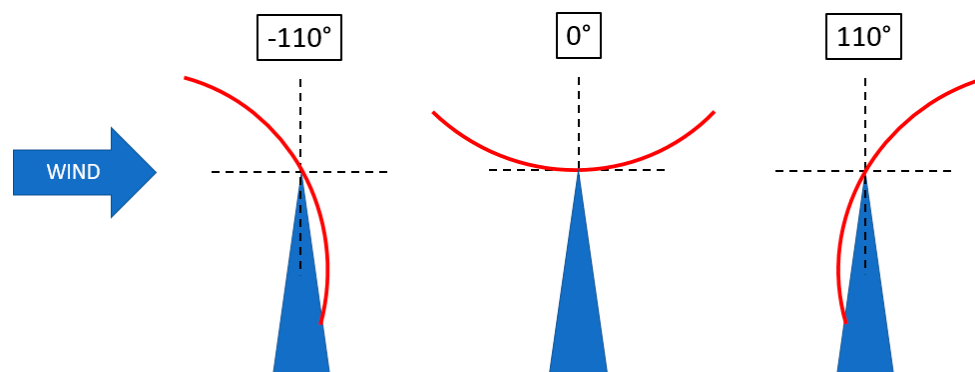


**Figure 5.** Notations for the definition of the rotation angle of the trough. The safety position is  $\pm 110^\circ$  (depending on wind direction).

To this aim, the following specific tests were performed:

- “Full rotation” test of the parabolic trough between the two limit values ( $\pm 110^\circ$ ). This test was performed to assess the behavior of the collector through the full range of possible rotation angles.
- “Rotation from service to recovery” test. The capability to quickly move from a service to a safety condition was assessed (exploiting a larger rotation speed).
- “Tracking” test: The correct movement of the trough as it followed the sun trajectory was verified.

All the test results were completely satisfactory because the trough demonstrated the ability to cover the desired angular range and to reach the safety position in a defined amount of time, respecting the design requirements.

### 2.2.3. Static Tests

The static tests were aimed at evaluating the behavior of the trough under different load typologies. More specifically, the following tests were performed:

- “Differential torsion” test. The behavior under a torsional load, obtained by imposing a rotation of one side of the prototype and keeping the other side fixed, was checked (Figure 6a).
- Distributed bending test. The behavior under a bending load obtained by imposing an equal rotation of both the tips of the prototype and using a 4 m long auxiliary structure, which constrained the central part of the prototype, in order to provide a reaction force, was investigated. This is a partially distributed load that involves the two central ribs (Figure 6b).
- “Concentrated bending” test. The behavior under a very localized concentrated bending load (160 mm-long) applied to one rib of the prototype was verified by using an auxiliary structure as a constraint (Figure 6c).
- “Wind load” test. The behavior applying a weight of 30 kg on the extremities of each rib, in order to simulate a distributed load that mimics some of the effects of the loads due to winds acting on the collector (Figure 6d).

The parabolic trough collector was specifically designed to ensure that, under the on-field loads, the maximum allowed deformation does not reduce the optical efficiency below some pre-defined threshold level. Therefore, the loads applied experimentally were selected to reach this limit condition and to verify the corresponding structural integrity.

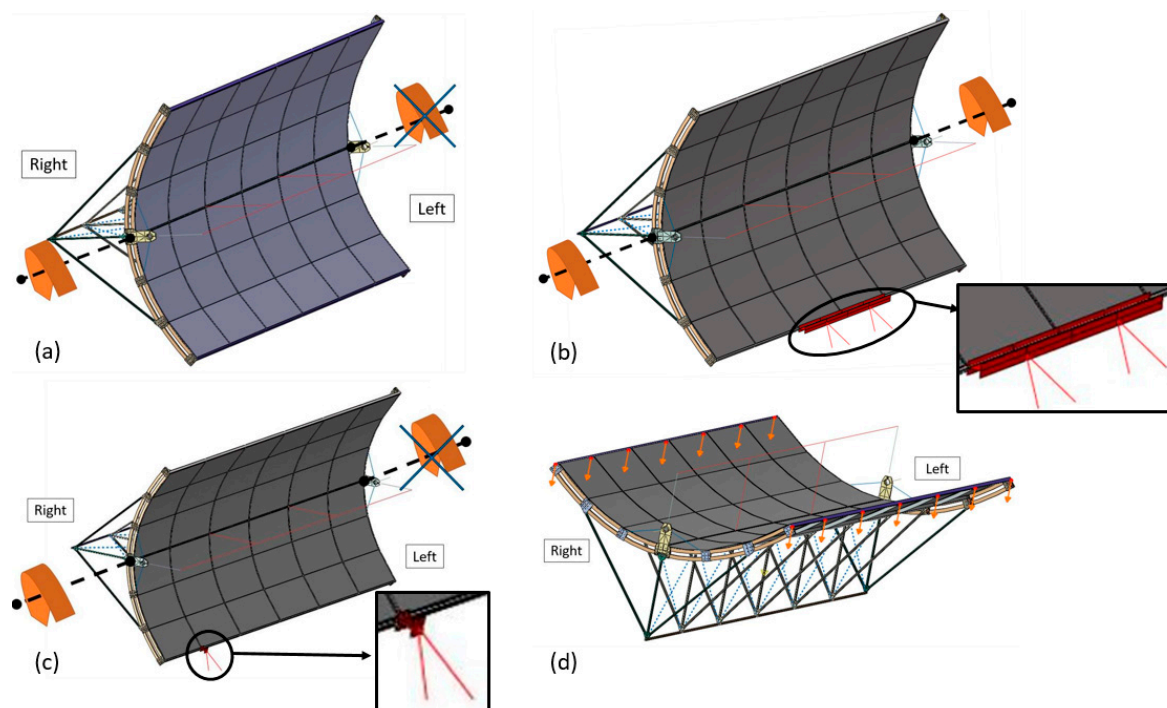


**Figure 6.** (a) Differential torsion test; (b) Distributed bending test; (c) Concentrated bending test; (d) Wind load test.

Figure 7 shows the locations of the measurement instruments adopted for the static tests, while Table 2 lists the instruments adopted for each test and their positions.

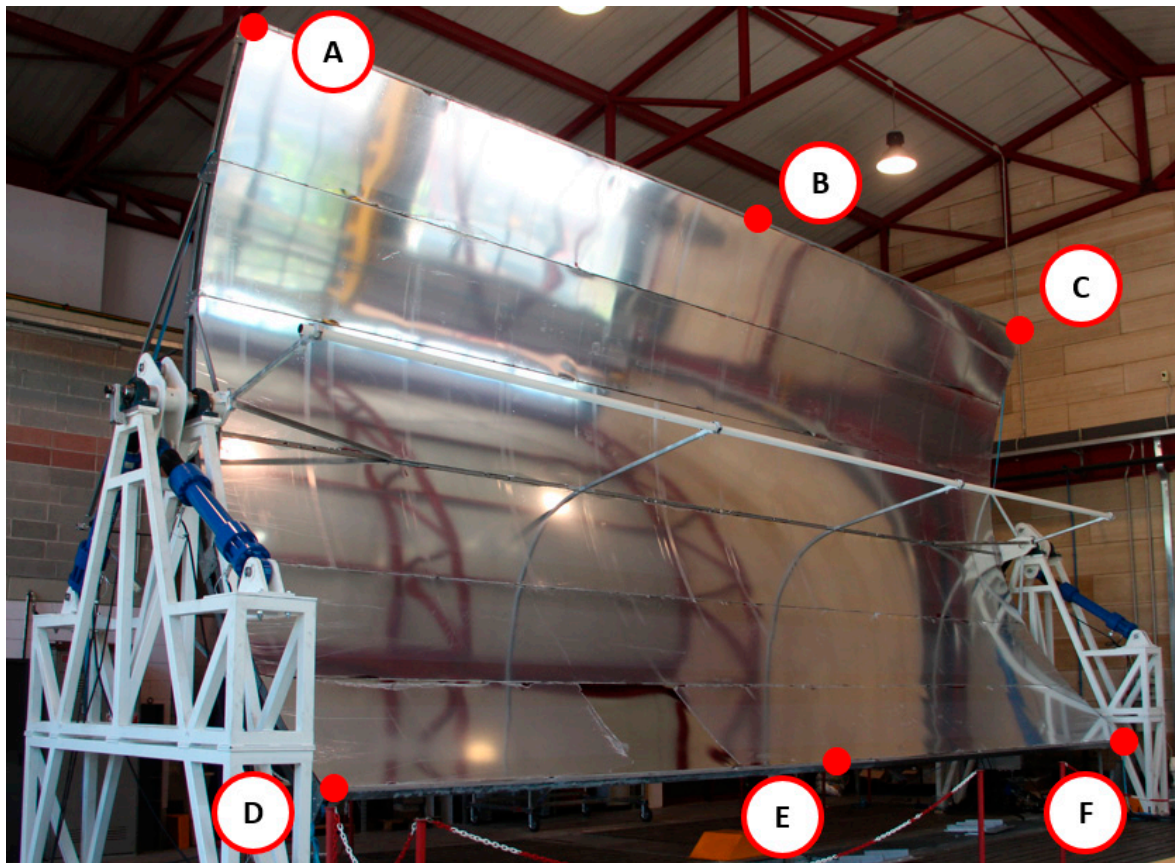


**Figure 7.** Location of the laser sensors and the cable transducers, see Table 2 for specifications of which sensor was used for each test.

**Table 2.** Measurement instrument position configurations adopted for the static tests.

Position	Differential Torsion Test	Distributed Bending Test	Concentrated Bending Test	Wind Load Test
Cable—Left (A)	X	X	X	
Cable—Middle (B)				X
Cable—Right (C)	X	X	X	
Laser—Left (D)		X	X	
Laser—Middle (E)	X	X		X
Laser—Right (F)	X	X	X	

### Differential Torsion Test

This test was performed in order to evaluate the behavior of the parabolic trough under a torsional load. More specifically, the main goal was to experimentally obtain the torsional stiffness of the collector prototype. The torsional stiffness is a critical parameter for a parabolic solar trough, since it is strictly related to the efficiency and the thermal performance of the collector, which, in field-scale installations, is often part of a longer row of collectors called the solar collector assembly (SCA). In order to investigate the torsional behavior of the prototype, the solar trough was fixed on one side, thereby blocking the actuators on one side in the desired position, whereas, on the other side, an increasing rotational angle was imposed by controlling the displacement of the other two actuators. The starting angle at which the prototype is rotated can be chosen arbitrarily, since only the effect of a rotation starting from the initial condition is of interest. The starting position of the prototype was set to an angle of  $90^\circ$ , with respect to the normal to the ground, since this configuration allowed for better laser and cable transducer placements in the proximity of the parabolic trough.

### Distributed Bending Test

This test was performed to evaluate the behavior of the parabolic trough prototype under a bending load. In order to apply a bending load, a service structure made of HE 160B steel beams was placed in correspondence to the central sections of the panel (between the 3rd and the 5th rib), imposing the same rotational angle to both sides of the parabolic trough, as shown in Figure 8a. The structure is made up of two bases fixed to the ground, on which was mounted an almost horizontal beam (4080 mm length), so that it could be put in contact with the trough ribs of interest. During the experimental test, the collector was rotated with an angle of  $100^\circ$ , with respect to the normal to the ground.

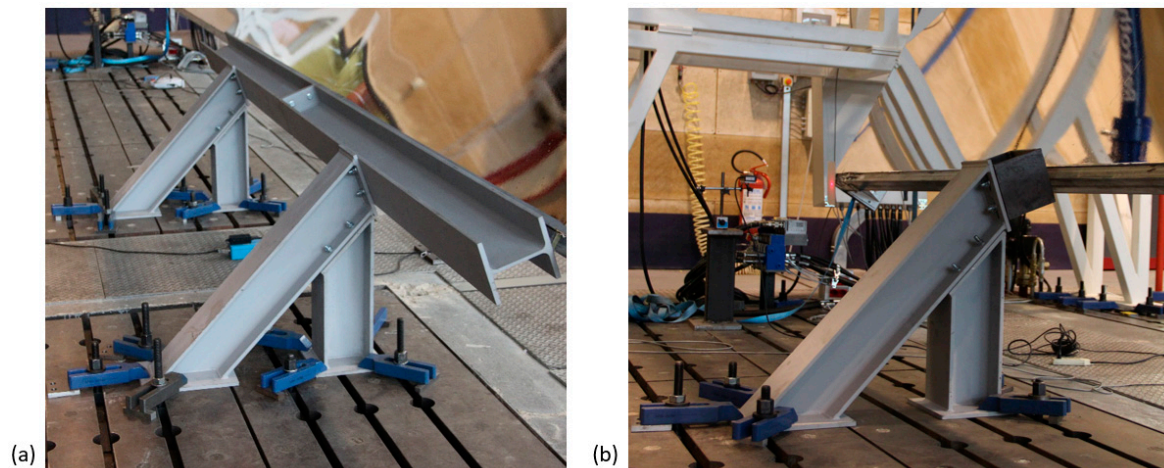


**Figure 8.** (a) Service structure for the distributed bending test; (b) Service structure for the concentrated bending test.

### Concentrated Bending Test

This test was aimed at evaluating the behaviour of the parabolic trough when subjected to a concentrated load. In order to analyze the bending behaviour of the prototype, a service structure made of HE 160B steel beams was placed in correspondence with the 2nd rib on the right side (Figure 8b), imposing a rotation angle on the right side, while the left one was kept fixed. Operatively, the configuration is similar to the differential torsion set up, but with the additional service structure at the lateral position, where the rotation is applied. During the experimental test, the collector was rotated with an angle of  $100^\circ$ , with respect to the normal to the ground.

### Wind Load Test

This test was aimed at evaluating the behaviour of the parabolic trough under a distributed load that mimics the load due to the actual wind on-site (acting on the front surface of the parabolic trough). A CFD analysis was carried out on a model of the collector that was rotated by a typical usage angle to calculate the bending moment acting on the structure when subject to a 50 km/h (13.9 m/s) wind. Then, equivalent concentrated forces applied at the concentrator tips were calculated to provide the same maximum bending moment. Finally, in order to mimic the effects of this bending load, a total of 14 weights were used (7 for each traverse, 1 for each rib tip), each one weighing 30 kg and linked to both ends of each inner rib and end rib. In this test, the collector was kept fixed in a fully horizontal condition ( $0^\circ$ , as shown in Figure 5), blocking the stroke of the actuators on both sides (and hence the rotation of the trough). In the test, the behaviours of the trough, both during the load phase (adding the weights) (Figure 9a) and unload phase (removing the weights) (Figure 9b), were examined.

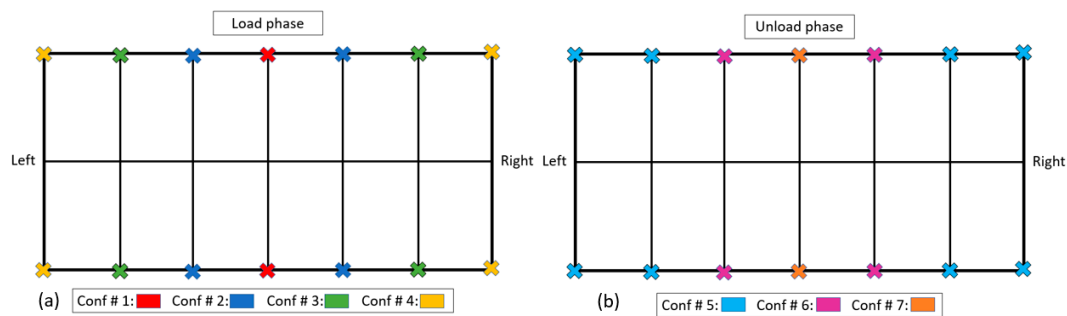


Figure 9. (a) Load phase configurations; (b) unload phase configurations.

#### 2.2.4. Fatigue Test

The fatigue experimental test was aimed at verifying the behaviour of the parabolic trough under variable loads, mimicking the effects of the winds acting on the collector in the solar field. A cyclic load was applied for 100,000 cycles with a frequency of 0.2 Hz, representing the estimated life cycle of the trough (25 years) in real operation conditions. During this experimental test, the collector was rotated with an angle of  $100^\circ$ , with respect to the normal to the ground, as previously done for the bending tests. To avoid the rotation of the solar trough, the stroke of the four actuators was kept fixed throughout the test. The load used for this test was similar to that applied during the distributed bending test, however, in this case, instead of using an auxiliary structure fixed to the ground in opposition to the rotation of the collector, a hydraulic actuator was used (Figure 10a). For this purpose, a 2 m steel beam was mounted on top of the actuator and placed in contact with the central area of the beam in the centre of the collector (Figure 10b). The actuator was controlled by a displacement control set-up to ensure that the chosen displacement implied the application of a certain desired load. Displacement control was chosen due to the local stabilization of the panels (of the parabolic trough) that occurs during each cycle and which could hardly be managed by a force control approach. The level of the load (peak to peak) was regularly checked in order to keep it constant and to compensate for the settling of the structure. The load was chosen with the aim to reproduce an effect similar to what occurs in the field due to wind action. In order to perform a severe test and assess the behaviour of the collector at the limit operating conditions, a load mimicking (in the selected part of the parabolic trough) the effect of a wind range was introduced, in which the maximum wind speed value was equal to the maximum value at which a collector should work in a solar field (50 km/h). The wind range cycle considered in the present work had an average value of 46 km/h, with an alternate wind speed of  $\pm 4$  km/h. The data related to the displacement and the reference force applied by the actuator are shown in Table 3. After 100,000 cycles, the parabolic collector showed no macroscopic failure/modification, confirming its reliability even after the application of a fatigue load.

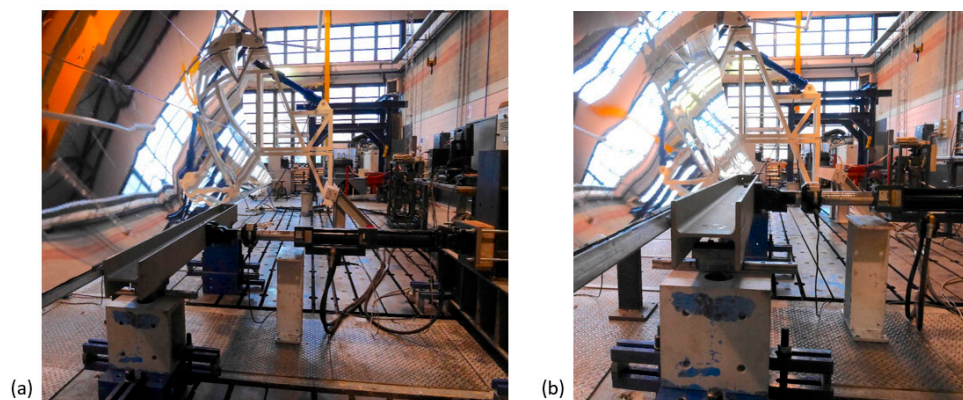


Figure 10. (a) Auxiliary structure and actuator used in the fatigue test; (b) Detail of the contact zone between the traverse and the beam.

**Table 3.** Actuator displacement and reference force.

	Actuator Displacement (mm)	Reference Load (N)
Maximum value	−80.5	−3400
Minimum value	−53.3	−1350
Average value	−66.9	−2375

### 3. Results

This section presents the outcomes of some of the tests performed among those described in the previous section, and more specifically, of those that were not just verifications of particular trough capabilities. Note that the actual values of angles and displacements in some of the plots have been normalized to their maximum values due to the confidentiality of the data.

#### 3.1. Differential Torsion Test

The results obtained from the differential torsion test are shown in Figure 11, in a graph representing the torsional moment (Nmm) versus the rotational angle ( $^{\circ}$ ). Note that this figure, and most of the following ones showing the results of the tests, does not show the actual values of some of the measured quantities, but rather their normalized values with respect to the maximum, due to confidentiality reasons. An expected small variation between the torque acquired at two sides was obtained. This variation is equal to approximately 2% of the value and can be attributed to the measurement uncertainty related to the encoder and the torsion strain gauges. The measured torsion stiffness was in good agreement with the expected stiffness planned during the design stage.

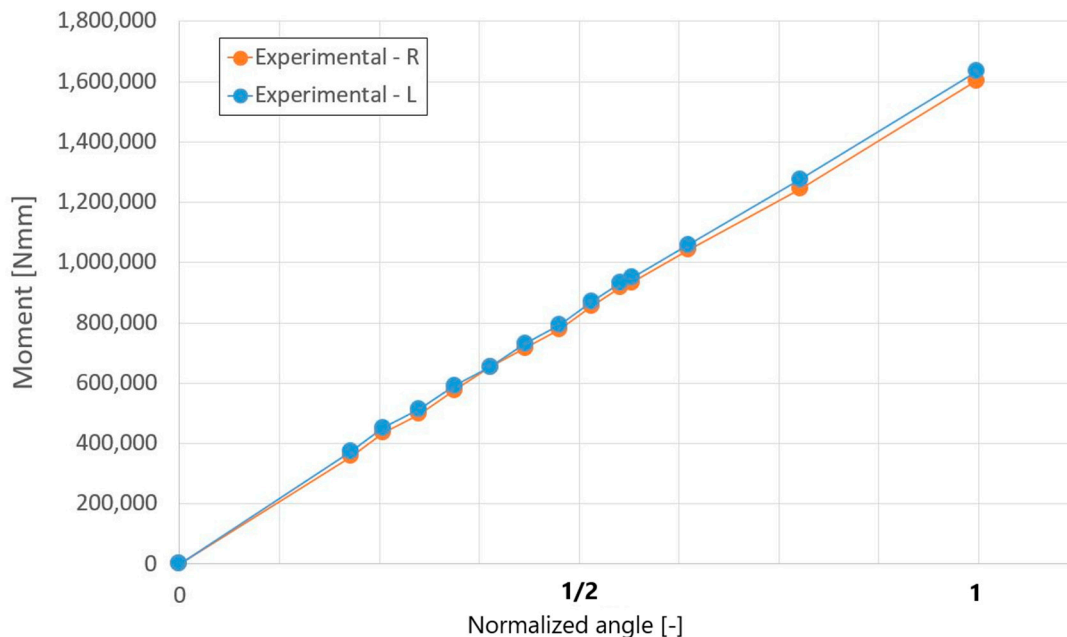


**Figure 11.** Torsional moment—Angle measured on the right (R) and left (L) sides. Actual values of angles have been normalized to the maximum value due to the confidentiality of the data.

The data collected from the SG show that the largest compression strain was achieved on strain gauge 32, placed on the left side of the back beam (Figure 12a). The largest tension strain, on the other hand, was achieved on strain gauge 30, placed on the first brace on the right side (Figure 12b).

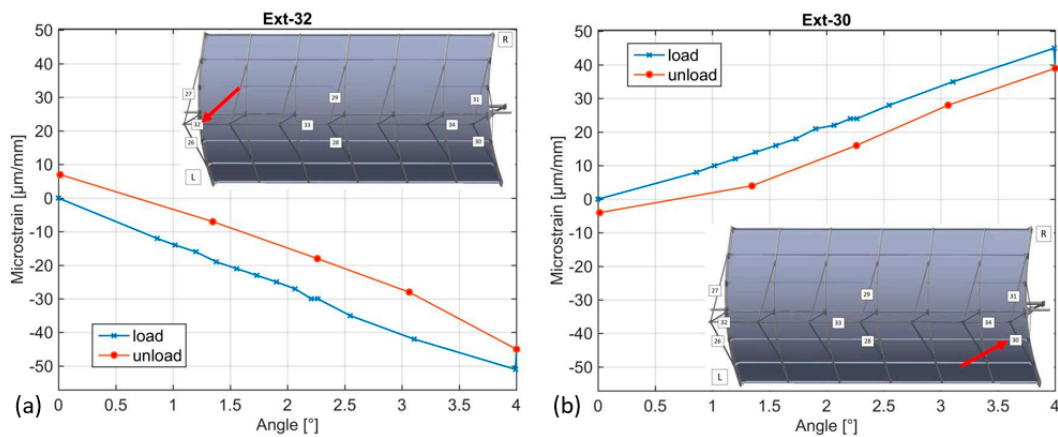


Figure 12. (a) Strain gauge 32; (b) Strain gauge 30.

The data acquired with the SG on the upper traverse show a gradient of the strain that passed from a positive value (tension), on the left side (Figure 13a), to a negative value (compression), on the right side (Figure 13b). The same gradient was also present on the lower traverse, but with tension on the right side (Figure 13d) and compression on the left one (Figure 13c). It is interesting to point out that, considering the strain gauges on the same side, the same value was present, but with the opposite sign (Figure 12 (a) vs. (c) and (b) vs. (d)). The data acquired by these strain gauges therefore show a double anti-symmetry in the strain distribution, with one symmetry axis along the collector axis and the other perpendicular to this one and passing by the central point of the structure. This result further confirms that the prototype was under a torsional load.

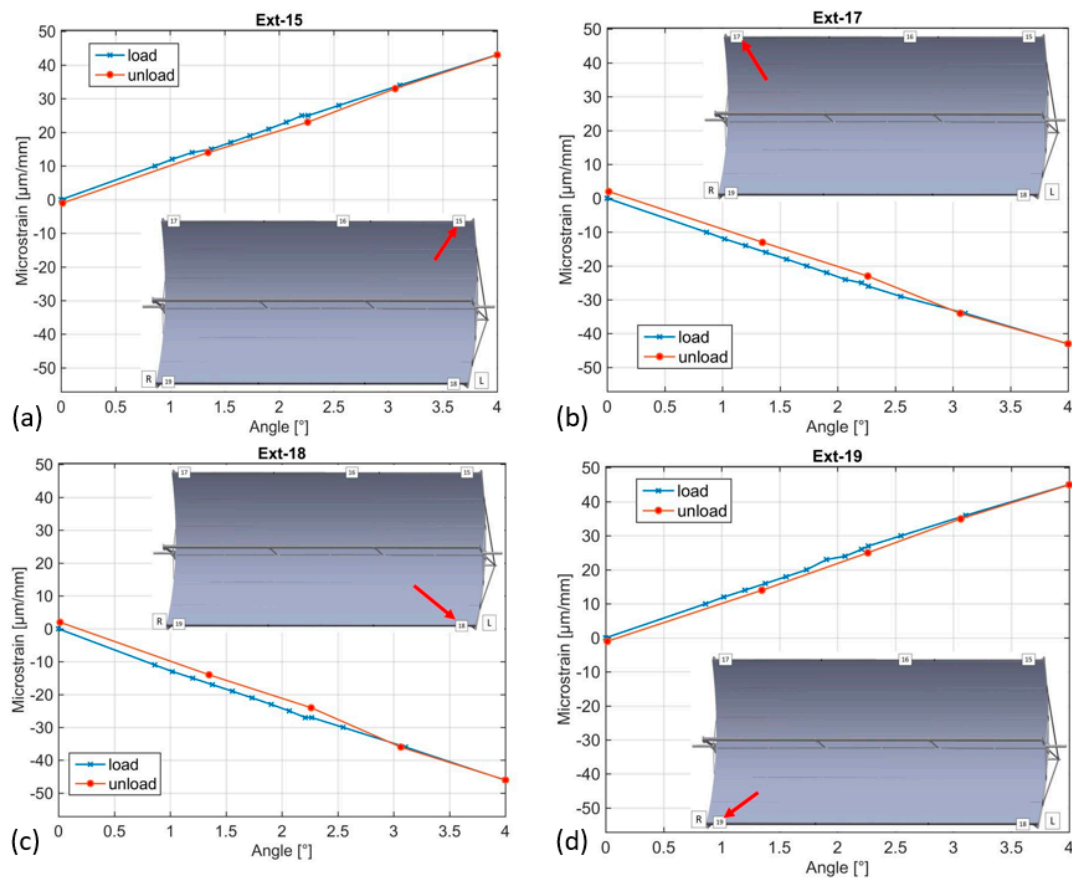
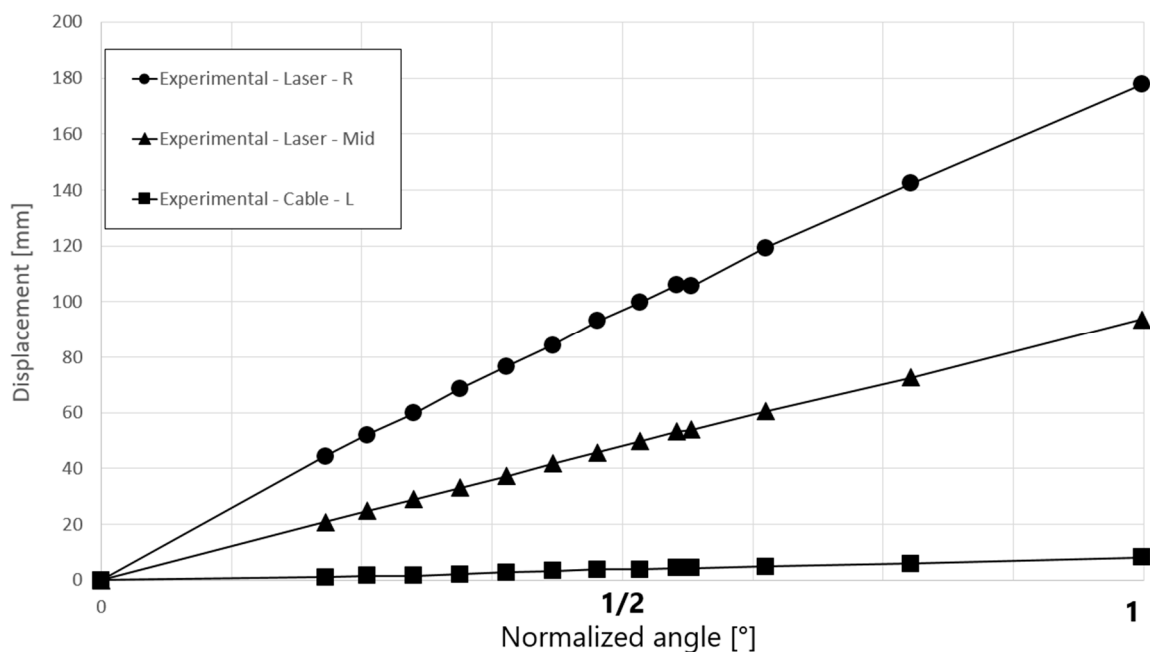


Figure 13. Measurements of (a) Strain gauge 15; (b) Strain gauge 17; (c) Strain gauge 18; (d) Strain gauge 19.

The results obtained from the lasers and the cable transducers placed around the collector are reported to give a comprehensive evaluation of the displacements. Initially, the data acquired from the different instruments were considered individually in order to assess the displacements measured along the structure. Then, for the right side of the parabolic trough (where it actually rotates), a comparison was performed to verify the agreement between the results obtained with the laser sensors and those obtained with the cable transducers. The displacement measurements obtained from the laser are plotted with respect to the rotation angle imposed to the collector in Figure 14. The displacement measured on the right side (Position F) is almost twice as high compared with the one obtained in the middle point of the traverse (Position E). This result agrees with the expectations and confirms the correct torsional behavior of the prototype. Furthermore, the signal from the cable transducer, located at Position A, is plotted with respect to the rotation angle in the same plot of Figure 14. The results show that the displacement values obtained on the left side (Position A), are much lower, i.e., approximately 10 mm. This behavior is consistent with the fact that this side of the trough was fixed, so that only a minimal displacement was measured (due to the compliance of the very small portion of the parabolic trough involved).



**Figure 14.** Displacement—Angle. Actual values of angles have been normalized to the maximum value due to the confidentiality of the data.

The comparison of the data obtained from the laser (Position F) with those from the cable transducer (Position C), both placed on the right side, forms the second evaluation of the trough. The results are plotted with respect to the rotation angle (Figure 15) and practically no difference, i.e., a few mm, is apparent between the instrument measurements. It can then be concluded that there was a correct rotation of this side of the prototype and that the measured results are consistent.

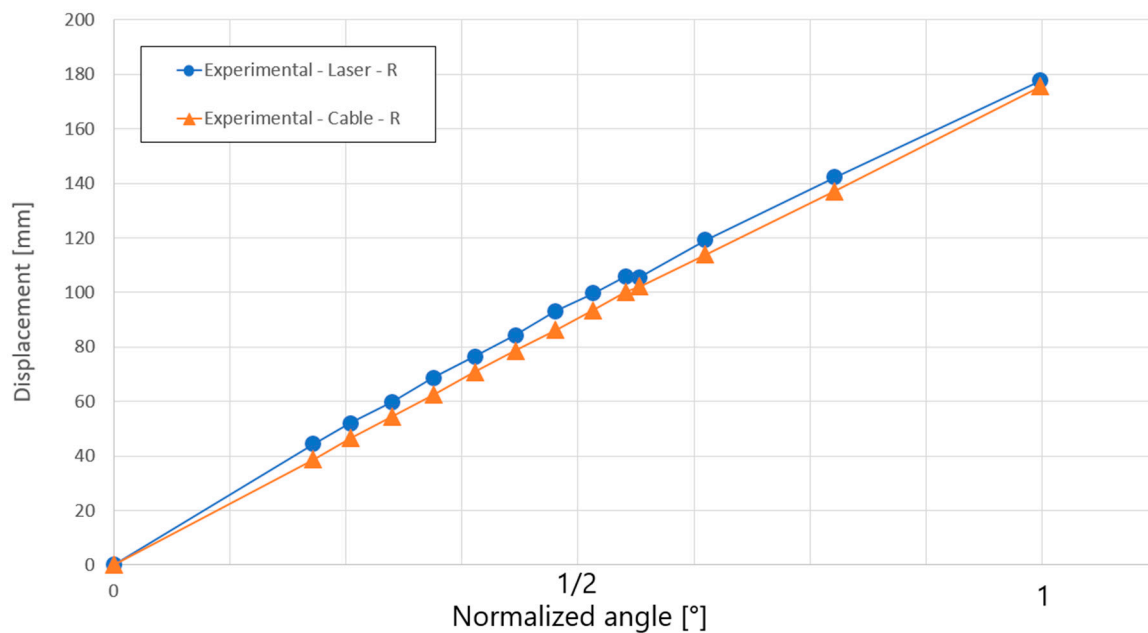


**Figure 15.** Comparison Laser—Cable transducer with respect to the angle. Actual values of angles have been normalized to the maximum value due to the confidentiality of the data.

### 3.2. Distributed Bending Test

The data observed with the SG show that the highest compression strain was achieved on the strain gauge 3, which was placed on the 4th rib. This result is in accordance with the type of load applied, since the area characterized by the highest stress/strain state was expected to be located close to the auxiliary structure (Figure 16a). The largest tension strain, on the other hand, was achieved on the strain gauge 16, placed on the upper traverse between the 4th and the 5th rib. Additionally, the result agrees with the expectations, since this strain gauge was placed in the central and most stressed zone of the collector (Figure 16b). Considering the measurements of strain gauges 1 (Figure 16c) and 5 (Figure 16d), which were placed on the 3rd and 5th ribs, the presence of a high compression strain value was also visible in these cases, even though the strain was lower than the one measured on the middle rib. This result indicates the correct response of the solar trough to the load imposed by the service structure. Moreover, the values of the different measurements are quite similar, confirming a symmetric behavior.

The measurements obtained with the lasers and the cable transducers placed around the collector show similar displacement values (Figure 17), confirming the symmetry of the structure and the load applied. Considering the measurements obtained with the cable transducers (Figure 18), the same symmetric behavior already highlighted by the data from the laser sensors was further confirmed. In both graphs the displacement is plotted with respect to the moment applied, and not, as before, with respect to the angle, since the rotation was found to be less than 1 degree and, thus, considered not very significant.

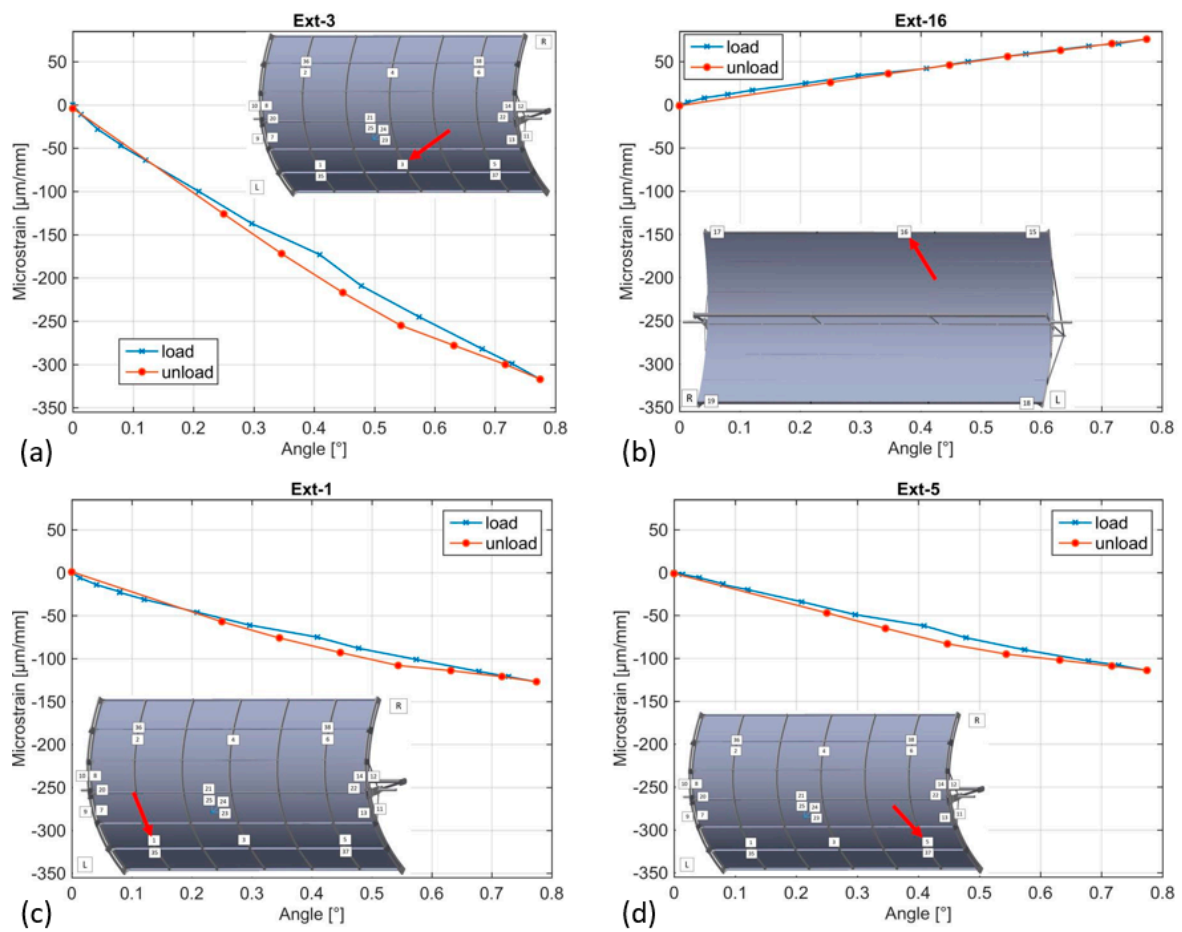


Figure 16. Measurements of (a) Strain gauge 3; (b) Strain gauge 16; (c) Strain gauge 1; (d) Strain gauge 5.

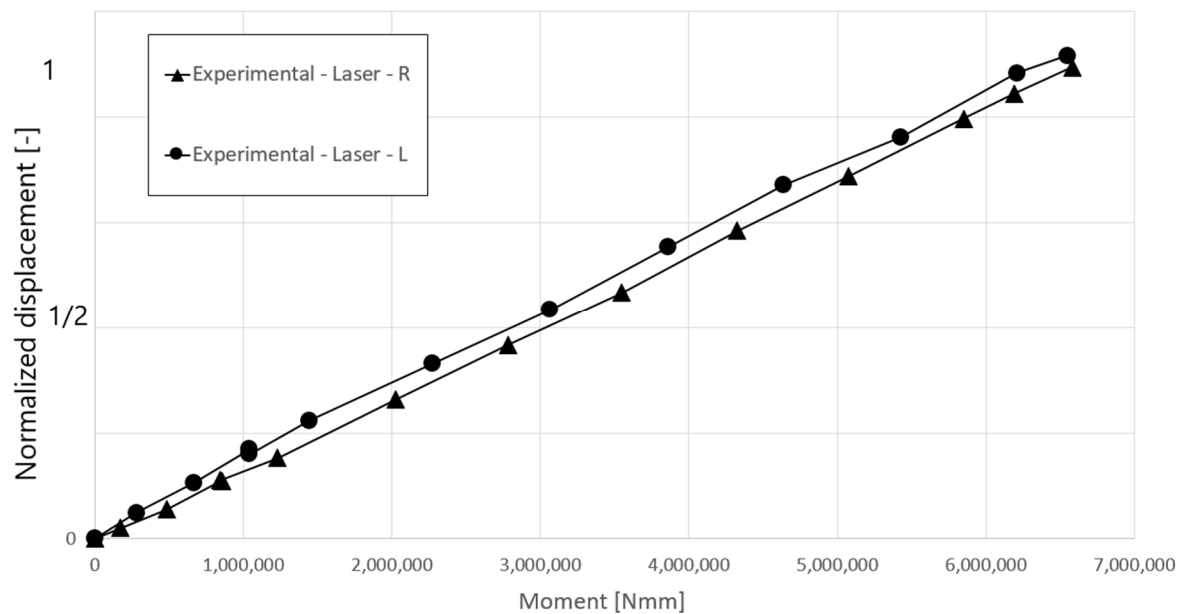
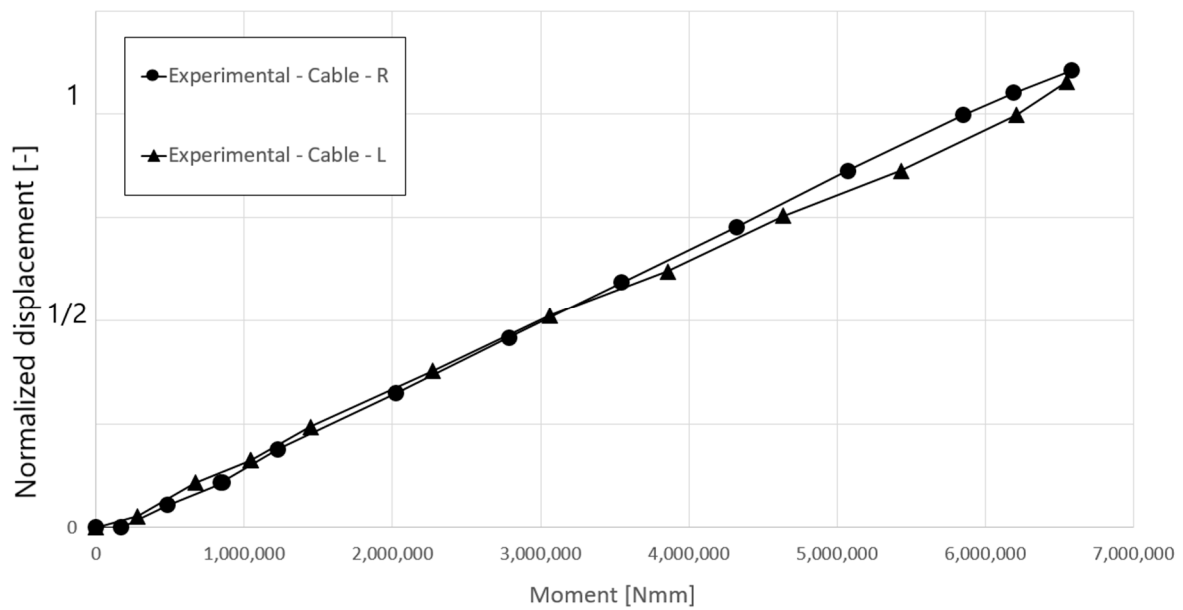


Figure 17. Displacement—Moment (Laser). Actual values of angles have been normalized to the maximum value due to the confidentiality of the data.



**Figure 18.** Displacement—Moment (Cable). Actual values of angles have been normalized to the maximum value due to confidentiality of the data.

### 3.3. Concentrated Bending Test

The data acquired by the SG show that the largest compression strain was reached on strain gauge 5, placed on the 2nd rib. This result was reasonably expected because the region with the largest stress/strain should be close to the auxiliary structure (Figure 19a). On the other hand, the highest tension strain was obtained on the strain gauge 37 (Figure 19b), placed on the joint connecting the 2nd rib with the panel. Both results agree with the expectations, since this strain gauge was placed in the most stressed zone of the collector. Taking into account the measurements taken with strain gauges 1 (Figure 19c) and 3 (Figure 19d), together with SG 5, all placed on the inner ribs, a strain gradient is visible with a maximum value in the area close to the service structure and decreasing values as the distance between the SG and this area increases.

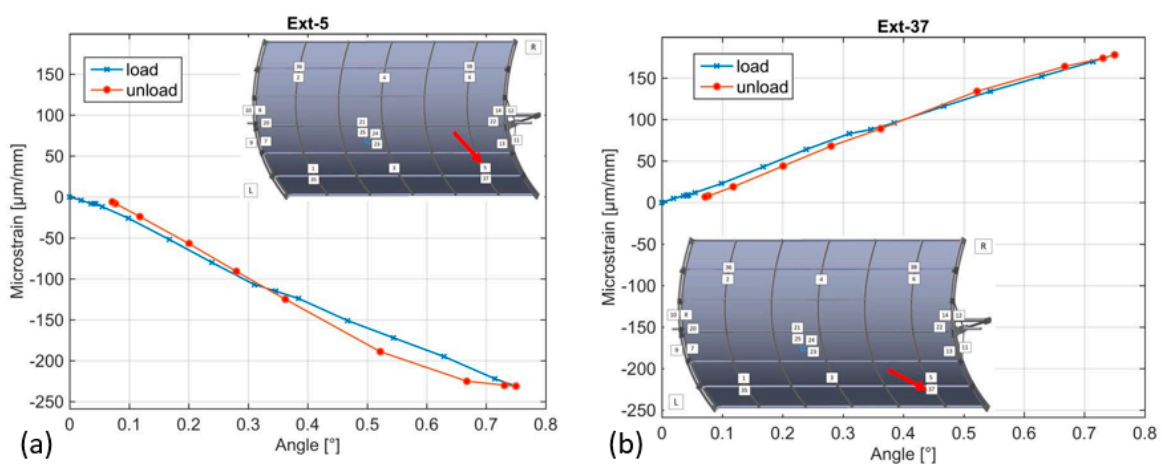


**Figure 19.** Cont.

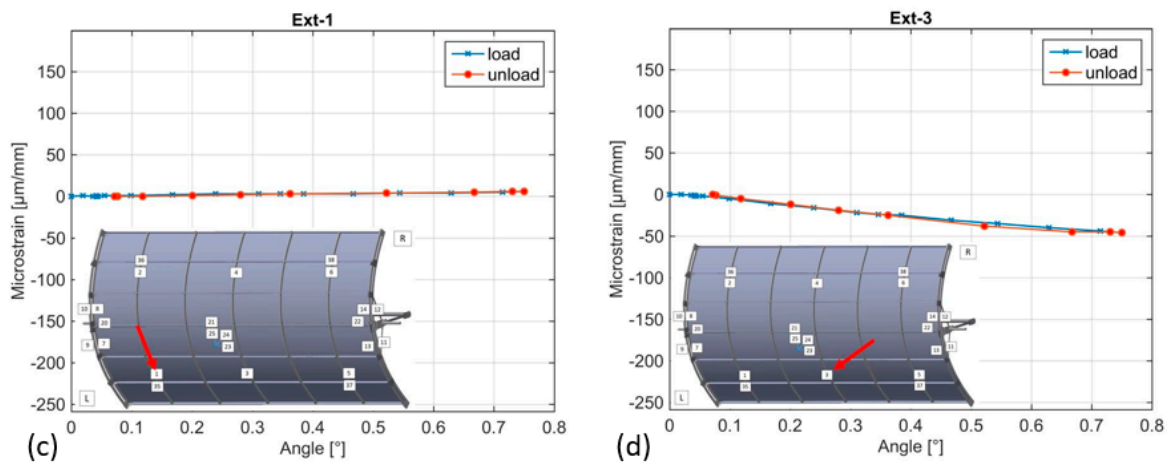


Figure 19. Measurements of (a) Strain gauge 5; (b) Strain gauge 37; (c) Strain gauge 1; (d) Strain gauge 3.

### 3.4. Wind Load Test

The observations with the SG show that the highest compression strain was achieved on strain gauge 3, which was placed on the 4th rib (Figure 20a). This result agrees with the typology of the load applied, since the zone with the largest stress/strain state is the central zone of the collector, where deflection is the highest. Considering strain gauges 1 (Figure 20b) and 5 (Figure 20c), placed on the 3rd and 5th ribs, a high compression strain was also measured in this zone, albeit lower than on the middle rib (SG 3). This result further demonstrates that the response of the solar trough when subjected to a distributed load agrees with the expectations. Indeed, the highest strain was present in the central part of the structure along its length (SG 3), while the other two values, related to more external SG with respect to the centreline, were lower and similar, also highlighting the symmetry of the behaviour.

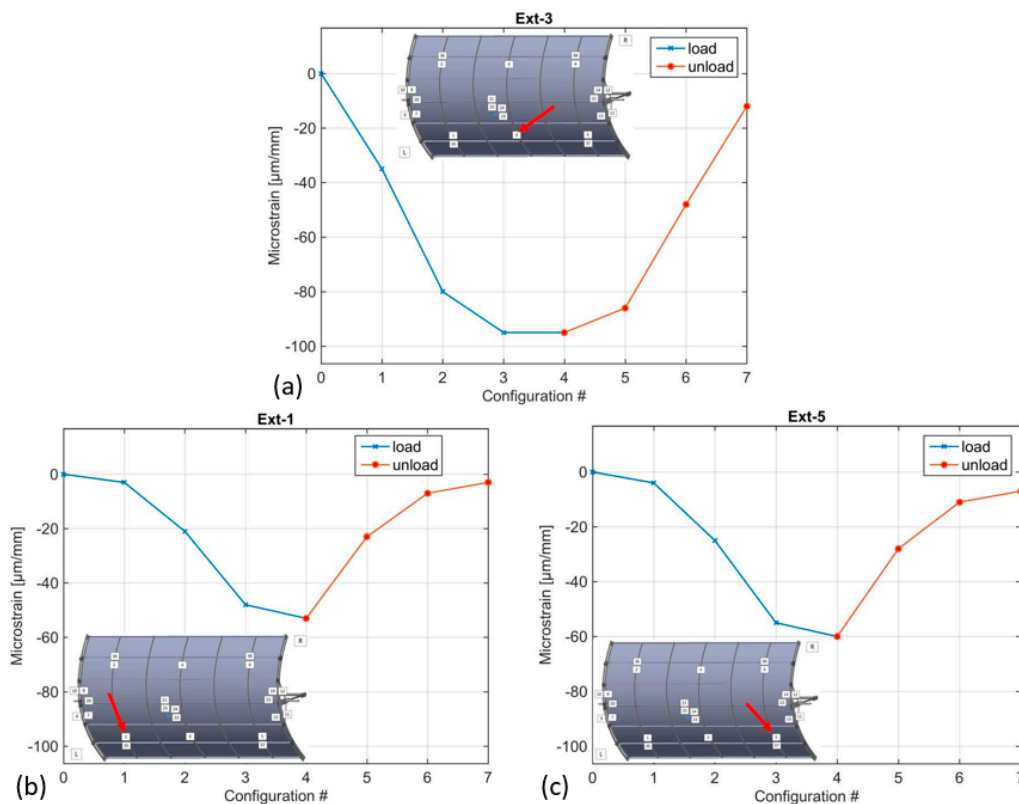


Figure 20. Measurements of (a) Strain gauge 3; (b) Strain gauge 1; (c) Strain gauge 5.

#### 4. Discussion

An experimental program was designed and carried out to assess the structure of an innovative parabolic trough and evaluate its performance. The tested parabolic trough collector presents a series of design innovations (especially the widespread use of adhesive resin and the lack of heavy stiffener auxiliary structures) resulting in a significant cost reduction and making it suitable for real on-site applications. However, design innovations exploited in this parabolic trough collector require rigorous experimental assessment to guarantee the reliability of the structure, and this was the goal of the present work. In the present work, investigations were conducted at both a global and local level. The results of the static tests showed that the trough could bear different types of applied loads and that the analysis of the data acquired from the strain gauges did not identify problematic regions. The evaluation of the torsional stiffness showed that an acceptable stiffness was achieved without the presence of heavy structures placed on the back of collector. This leads to a great reduction of both the weight and the complexity of the system. Furthermore, the structure was able to accomplish a fatigue test under a load larger than those typical of the most critical on-site conditions. The experimental activity presented in this work has proven that the innovative design of the parabolic trough can be successfully applied for power production scale use and that the innovations developed in the design stage are not only feasible, but also very effective in terms of performance.

**Author Contributions:** A.G., L.A., M.F., F.C., A.M., M.G., L.C., C.B.V., S.C. conceptualization, M.G., L.C., C.B.V.; methodology, A.G., L.A., M.F., F.C., A.M., M.G., L.C., C.B.V., S.C.; software, A.G., L.A., M.F., S.C.; formal analysis, A.G., L.A., M.F., S.C.; investigation, A.G., L.A., M.F., F.C., A.M., M.G., L.C., C.B.V., S.C.; writing—original draft preparation, A.G. and S.C.; writing—review and editing, F.C., A.M., L.C., C.B.V., S.C.; supervision, M.G., L.C., C.B.V.; funding acquisition, M.G., L.C., C.B.V.

**Funding:** This research was partially funded by Eni S.p.A, in the framework of the agreement with Politecnico di Milano n. 4400007601.

**Acknowledgments:** The parabolic trough designed and constructed at the laboratory of the Politecnico di Milano in 2016 was developed by the joint effort of Politecnico di Milano, Massachusetts Institute of Technology and Eni.

**Conflicts of Interest:** The authors declare no conflicts of interest.

#### References

1. Barlev, D.; Vidu, R.; Stroeve, P. Innovation in concentrated solar power. *Sol. Energy Mater. Sol. Cells* **2011**, *95*, 2703–2725. [[CrossRef](#)]
2. Jebasingh, V.K.; Herbert, G.M. A review of solar parabolic trough collector. *Renew. Sustain. Energy Rev.* **2016**, *54*, 1085–1091. [[CrossRef](#)]
3. Răboacă, M.S.; Badea, G.; Enache, A.; Filote, C.; Răsoi, G.; Rata, M.; Lavric, A.; Felseghi, R.-A. Concentrating Solar Power Technologies. *Energies* **2019**, *12*, 1048. [[CrossRef](#)]
4. Kumaresan, G.; Sudhakar, P.; Santosh, R.; Velraj, R. Experimental and numerical studies of thermal performance enhancement in the receiver part of solar parabolic trough collectors. *Renew. Sustain. Energy Rev.* **2017**, *77*, 1363–1374. [[CrossRef](#)]
5. Uzair, M.; ur Rehman, N.; Raza, S.A. Probabilistic approach for estimating heat fluid exit temperature correlation in a linear parabolic trough solar collector. *J. Mech. Sci. Technol.* **2018**, *32*, 447–453. [[CrossRef](#)]
6. Soudani, M.E.; Aiadi, K.E.; Bechki, D.; Chihi, S. Experimental and theoretical study of Parabolic trough collector (PTC) with a flat glass cover in the region of algerian sahara (Ouargla). *J. Mech. Sci. Technol.* **2017**, *31*, 4003–4009. [[CrossRef](#)]
7. Saucedo, D.; Velázquez, N.; García-Valladares, O.; Beltrán, R. Numerical simulation and design of a parabolic trough solar collector used as a direct generator in a solar-GAX cooling cycle. *J. Mech. Sci. Technol.* **2011**, *25*, 1399–1408. [[CrossRef](#)]
8. Zamparelli, C. Storia, Scienza e Leggenda Degli Specchi Ustori di Archimede. Available online: <https://www.gses.it/pub/specchi1.pdf> (accessed on 21 November 2019).
9. IRENA. *Renewable Power Generation Cost in 2014*; IRENA: Abu Dhabi, UAE, 2015.

10. Geyer, M.; Lüpfer, E. EUROTROUGH—Parabolic Trough Collector Developed for Cost Efficient Solar Power Generation. In Proceedings of the 11th SolarPACES International Symposium on Concentrated Solar Power and Chemical Energy Technologies, Zurich, Switzerland, 4–6 September 2002.
11. Energy.Gov | SunShot Initiative. Available online: <https://energy.gov/eere/sunshot/sunshot-initiative> (accessed on 21 November 2019).
12. Mokheimer, E.M.A.; Dabwan, Y.N.; Habib, M.A.; Said, S.A.M.; Al-sulaiman, F.A. Techno-economic performance analysis of parabolic trough collector in Dhahran, Saudi Arabia. *Energy Convers. Manag.* **2014**, *86*, 622–633. [[CrossRef](#)]
13. Slocum, A.H.; Campbell, R.B. Low Cost Parabolic Cylindrical trough for Concentrated Solar Power. U.S. Brevetto US20170082322, 23 March 2017.
14. Kötter, J.; Riffelmann, K.-J.; Decker, S.; Fellmuth, J.; Macke, A.; Nava, P.; Weinrebe, G.; Schiel, W.; Steindorf, A.; Dracker, R. Heliotrough—One Year Experience with the Loop in a Commercial Solar Power Plant. In Proceedings of the SolarPACES 2010 Conference, Perpignan, France, 21–24 September 2010.
15. Rubia, S.V.; Schramm, M.; Yildiz, H.; Marcotte, P. Construction and Thermal Efficiency Test of 145m and 165m SpaceTube<sup>®</sup> Large-Aperture Parabolic Trough Collector Prototypes. *AIP Conf. Proc.* **2016**, *1734*. [[CrossRef](#)]
16. Praveen, R.P.; Abdul Baseer, M.; Awan, A.B.; Zubair, M. Performance Analysis and Optimization of a Parabolic Trough Solar Power Plant in the Middle East Region. *Energies* **2018**, *11*, 741. [[CrossRef](#)]
17. Fernandez-Garcia, A.; Zarza, E.; Valenzuela, L.; Perez, M. Parabolic trough solar collectors and their applications. *Renew. Sustain. Energy Rev.* **2010**, *14*, 1695–1721. [[CrossRef](#)]
18. Gunther, M.; Joemann, M.; Csambor, S. Parabolic Trough Collector. In *Advanced CSP Teaching Materials*; Deutsches Zentrum für Luft- und Raumfahrt e.V.: Stuttgart, Germany, 2011; Chapter 5.
19. Price, H.; Lüpfer, E.; Kearney, D.; Zarza, E.; Cohen, G. Advances in Parabolic Trough Solar Power Technology. *J. Sol. Energy Eng.* **2002**, *124*, 109–125. [[CrossRef](#)]
20. Marcotte, P.; Manning, K. Development of an advanced large-aperture parabolic trough collector. *Energy Procedia* **2013**, *49*, 145–154. [[CrossRef](#)]
21. Cardamone, S. Ottimizzazione Strutturale di un Collettore Solare Parabolico Mediante la Tecnologia Dell'incollaggio. Master's Thesis, Politecnico di Milano, Milan, Italy, 2013.
22. Crescenzo, C.D. Numerical, Experimental and NDT Analyses on Adhesively Bonded Joints of a Parabolic Solar Trough. Master's Thesis, Politecnico di Milano, Milan, Italy, 2017.
23. Giannuzzi, G.M.; Majorana, C.E.; Miliozzi, A.; Salomoni, V.; Nicolini, D. Structural Design Criteria for Steel Components of Parabolic-Trough Solar Concentrators. *J. Sol. Energy Eng.* **2007**, *129*, 382–390. [[CrossRef](#)]
24. Salomoni, V.A.; Majorana, C.E.; Giannuzzi, G.M. New Trends in Designing Parabolic trough Solar Concentrators and Heat Storage Concrete Systems in Solar Power Plants. In *Solar Energy*; 2010; pp. 268–292. Available online: <https://www.intechopen.com/books/solar-energy/new-trends-in-designing-parabolic-trough-solar-concentrators-and-heat-storage-concrete-systems-in-so> (accessed on 21 November 2019).

